

Force Measurements Using Capillary Instabilities

ULLRICH STEINER

Department of Physics, University of Cambridge, Cambridge CB3 0HE, United Kingdom

Received 4 August 2005; revised 8 September 2005; accepted 8 September 2005

DOI: 10.1002/polb.20631

Published online in Wiley InterScience (www.interscience.wiley.com).

ABSTRACT: This article reviews some recent experimental studies on film instabilities. Since surface instabilities of planar films are driven by destabilizing interfacial pressures, the patterns that form in thin films are a signature of these interfacial forces. The direct correspondence of pattern selection and the underlying destabilizing pressures provides a way to quantitatively determine these interface potentials. This principle is documented for three different film destabilization mechanisms: van der Waals forces, forces caused by an applied electric field, and forces that arise from the confinement of thermal molecular motion in the film. ©2005 Wiley Periodicals, Inc. *J Polym Sci Part B: Polym Phys* 43: 3395–3405, 2005

Keywords: films; morphology; surfaces

INTRODUCTION

The study of capillary surface instabilities has a long history. The first systematic discussion of the interplay of liquid morphologies and surface tension dates back to 1878 when Lord Rayleigh provided a model for the decay of a liquid cylinder into drops.^{1,2} As opposed to liquid cylinders, planar surfaces of bulk liquids are intrinsically stable with respect to small perturbations, such as capillary waves. When perturbed by an externally applied destabilizing force, however, surface instabilities that exhibit a characteristic lateral length scale are observed.^{3,4} This is particularly easy to observe for electrostatic interactions of the surface with its environment.⁵ First observations of the deformation of a liquid surface by an electric field date back to the 17th century, with more detailed description from Lord Rayleigh in 1882.⁶

The so-called electrohydrodynamic (EHD) instability has since then captured the imagination of physicists and engineers. Based on an experiment by Swan in 1897,⁷ in which a resin film was

destabilized by an electrical discharge, the use of EHD instabilities in a recording techniques was suggested by a number of authors in the 1960s.^{8,9}

Although EHD and magnetohydrodynamic instabilities on macroscopic bodies of liquids were extensively studied in the 1960s,⁵ this field of research is recently receiving renewed attention.^{10–23} Although the restoring force of surface waves with sufficiently long wavelengths is gravity, microscopic surface perturbations are stabilized by the surface tension. The dewetting of polymer thin films has been a recent focus of attention, because the instabilities of thin layers reveal forces and rheological properties of a macromolecular liquid in confinement.²⁴ The control of the pattern formation caused by capillary surface instabilities gives rise to novel lithographic techniques.^{10–12,14,25,26}

The pattern formation mechanism of planar liquid surfaces in the presence of a destabilizing potential is well described by a simple theoretical framework, the so-called linear stability analysis,^{3,4} which provides a quantitative characterization of the pattern formation process in the limit, where the surface wave amplitude is much smaller than the wavelength. In this long wavelength limit, a simple universal relation connects the pattern selection with the gradient of the

Correspondence to: U. Steiner (E-mail: www.phy.cam.ac.uk/steiner)

Journal of Polymer Science: Part B: Polymer Physics, Vol. 43, 3395–3405 (2005)
©2005 Wiley Periodicals, Inc.

destabilizing surface pressure. This characterization of surface instabilities in terms of their characteristic wavelength allows therefore to deduce the destabilizing potential. This enables quantitative force measurements in which the morphologies of destabilized films are studied as a function of the parameters that modulate the applied destabilizing potential. This article reviews several recent examples in which this principle was applied.

CAPILLARY SURFACE INSTABILITIES

Planar liquid surfaces are stable, because any surface perturbation leads to an increase in surface area. This argument applies, however, only for the time-averaged surface structure. Thermal motion of the molecules on both sides of the liquid interface continuously excites a spectrum of capillary waves, which is entirely overdamped.²⁷ An additional force that acts at the liquid surface couples to the capillary wave spectrum. The consequences of such an additional potential can be predicted by a linear stability analysis. Following Vrij³ and Brochard-Wyart and Daillant,⁴ the capillary wave spectrum is modeled in a one-dimensional representation (Fig. 1)

$$h(x, t) = h_0 + h_a \exp\left(iqx + \frac{t}{\tau}\right) \quad (1)$$

This assumes a thin film with an averaged thickness h_0 , with a superposed spectrum of sinusoidal waves with wavevector q and amplitude h_a . The time constant τ determines the temporal evolution of each q -mode, with positive (negative) values of τ corresponding to an amplification (damping) of the mode. The modulation of the surface

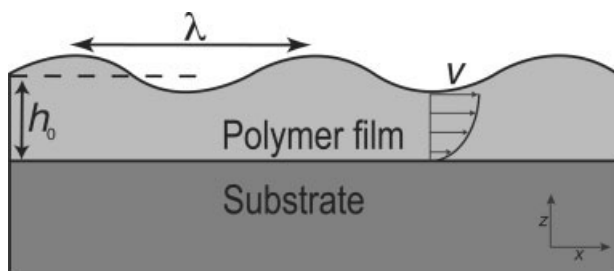


Figure 1. Schematic representation of a capillary instability. In the presence of a destabilizing pressure gradient, the initially flat surface develops a surface wave with a well-defined wavelength λ . The material transport inside the layer is modeled by a parabolic velocity profile v .

requires a material transport inside the film. In the thin film limit, where convection is suppressed, the Navier–Stokes equation can be considerably simplified by using the so-called lubrication approximation.²⁸ The vertical component (along the z -direction) of the flow profile $v(x)$ is neglected and its in-plane component (x -direction) has a Poiseuille-type parabolic dependence

$$\eta \frac{\partial^2 v}{\partial z^2} = \frac{\partial p}{\partial x} \quad (2)$$

where η is the viscosity. Assuming a zero-velocity boundary condition at the substrate interface and the disappearance of tangential stresses at the free surface

$$\eta v = \frac{1}{2} \frac{\partial p}{\partial x} (z^2 - 2hz) \quad (3)$$

The overall lateral flux is

$$\eta j = -\frac{h^3}{3} \frac{\partial p}{\partial x} \quad (4)$$

with $j = 1/h \int_0^h v \, dz$. When nonvolatile, incompressible liquids are used, mass-conservation must be obeyed. In one dimension,

$$\frac{\partial h}{\partial t} + \frac{\partial j}{\partial x} = 0 \quad (5)$$

The combination of eqs 4 and 5 lead to the equation of motion of the film

$$\frac{\partial h}{\partial t} = \frac{1}{3\eta} \frac{\partial}{\partial x} \left(h^3 \frac{\partial p}{\partial x} \right) \quad (6)$$

In thin films, the main restoring forces stems from the Laplace pressure $p_L = -\gamma \partial^2 h / \partial x^2$. Without loss of generality, $p = p_L + p_{\text{int}}$, where p_{int} contains all additional pressure terms that act at the liquid surface.

The equation of motion (eq 6) is solved using the ansatz from eq 1. The resulting differential equation is solved in a linear approximation (only terms linear in h_a are considered). This leads to the dispersion relation

$$\frac{1}{\tau} = -\frac{h_0^3}{3\eta} \left(\gamma q^4 + \frac{\partial p_{\text{int}}}{\partial h} \right) \quad (7)$$

Depending on the sign of $\partial p_{\text{int}} / \partial h$, a part of the q -spectrum may be amplified (positive values of τ). Because of the exponential nature of the amplification mechanism, the fastest growing mode (smallest positive value of τ) will eventually dominate. The pattern selection is therefore given by

the maximum of eq 7

$$q_m^2 = -\frac{1}{2\gamma} \frac{\partial p_{\text{int}}}{\partial h} \quad (8)$$

In terms of the interfacial potential $\phi = \int p \, dh$ and the wavelength of the instability $\lambda = 2\pi/q$, this can also be written as

$$\lambda = \sqrt{8\pi^2\gamma \left(\frac{\partial^2 \phi_{\text{int}}}{\partial h^2} \right)^{-1}} \quad (9)$$

Although equations of the type eq 9 are well known, it is the intriguing simplicity of this relation that makes it useful to measure forces on a nanometer scale: the selected mode of a surface instability q_m directly reflects the strength of the destabilizing pressure gradient. An experiment in which the parameters that govern p_{int} are systematically varied therefore provides a way to quantitatively measure p_{int} . This review illustrates a number of recent examples, which made use of this principle.

VAN DER WAALS FORCES

The most discussed case of spontaneous film break-up is caused by a van der Waals conjoining pressure. In thin film geometry, it is given by²⁹

$$p_{\text{vdW}} = \frac{A}{6\pi h^3} \quad (10)$$

$$p_{\text{vdW}} = \frac{B}{h^4} \quad (11)$$

for nonretarded and retarded van der Waals forces, respectively. The Hamaker constants A and B can be predicted either by microscopic models (based on the polarizations of individual atoms) or by an electromagnetic frequency average over the macroscopic dielectric properties of the film and the two bounding media.³⁰ For polymers, a number of approximations have been used, which typically provide a good approximation for more accurate models.³⁰ One often used approximation is the Lifshitz formula for A ²⁹

$$A \approx \frac{3}{4} kT \left(\frac{\varepsilon_s - \varepsilon_f}{\varepsilon_s + \varepsilon_f} \right) \left(\frac{\varepsilon_a - \varepsilon_f}{\varepsilon_a + \varepsilon_f} \right) + \frac{3h\nu_e}{8\sqrt{2}} \frac{(n_s^2 - n_f^2)(n_a^2 - n_f^2)}{\sqrt{n_s^2 + n_f^2} \sqrt{n_a^2 + n_f^2} (\sqrt{n_s^2 + n_f^2} + \sqrt{n_a^2 + n_f^2})} \quad (12)$$

with the dielectric constants ε_i and refractive indices n_i of the three media, and $h\nu_e$ the energy

corresponding to the main electronic UV absorption frequency $\nu_e \approx 3 \times 10^{15}$ Hz. The indices correspond to air, film, and substrate, respectively. Since the first term of eq 12 contributes only $\sim 10\%$, the Hamaker constant can be approximated in terms of the refractive indices of the three media. For thin enough films (< 10 nm), retardation effects are small and can be neglected. It should be noted that all predictions of A are subject to a significant uncertainty³⁰ and we therefore expect the values obtained from eq 12 to be on the correct order of magnitude only.

Since eq 10 diverges for $h \rightarrow 0$, a short-ranged repulsive potential must be included for small film thicknesses. It was derived using self-consistent field calculations by Müller et al.³¹

$$\phi_s(h) = \frac{c}{h^8} \quad (13)$$

Although essential for an overall consistent description of thin films, ϕ_s is overpowered by the van der Waals potential for $h > 2$ nm (see Fig. 2), and must therefore be considered only for extremely thin films.

A convincing experimental analysis of polymer film instabilities in the framework of eq 9 was performed by Seemann, Jacobs, and Herminghaus (SJH).²⁴ By carefully measuring the instability wavelength λ versus the thickness h of a polystyrene (PS) film, they were able to construct the functional form of the vdW disjoining potential as a function of h . From the variation of λ with h , the second derivative of the potential is obtained from eq 9 [Fig. 2(a,b)]. After fitting the data to eq 9 using eq 10 (also including ϕ_s from eq 13), the fitted curves were integrated to give $\phi(h)$ [Fig. 2(c)].

Their experimental system is interesting because of the substrate boundary condition. In one of their experiments, they used a silicon wafer that was covered by a 2.4-nm thick oxide layer. The effective disjoining pressure of a polymer film on such a composite substrate is strongly dependent on the film thickness. Thin films are dominated by the destabilizing effect of the low refractive index oxide layer, while thicker PS films are stable due to the stabilizing vdW disjoining pressure exerted by the Si substrate. At the crossover film thickness, the two effects cancel each other and the effective vdW disjoining pressure is zero. This is clearly visible by the divergence of the λ versus h curve in Figure 2(a).

The SJH experiments are a convincing example that a relatively simple dewetting experiment can be used to quantitatively measure interfacial

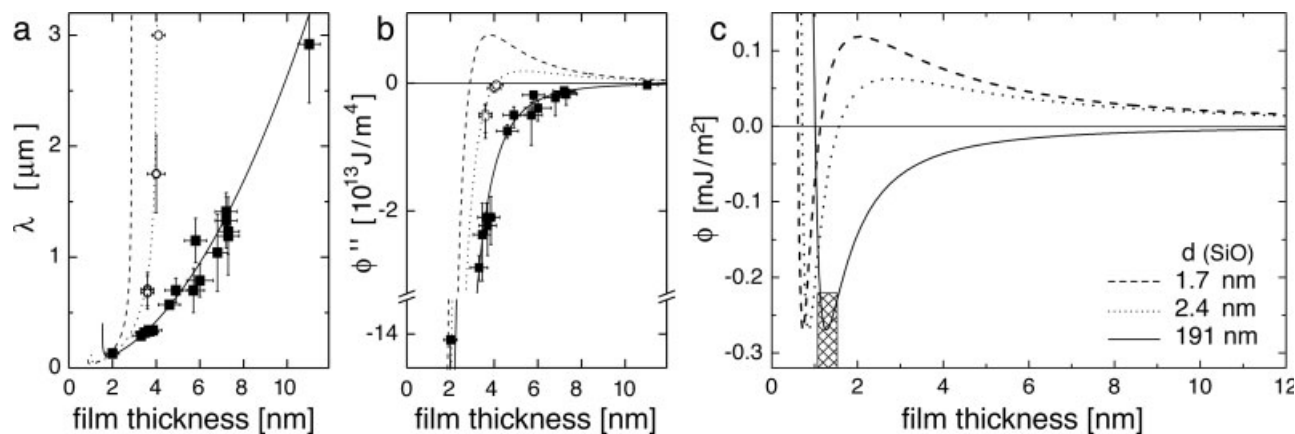


Figure 2. Experimental measurement of an interfacial potential that led to the dewetting of thin PS films by Seemann et al.²⁴ Silicon substrates with oxide layers of three different thicknesses d (SiO) were used. PS films of all thicknesses were found to be unstable on the thickest oxide layer. For thinner oxide layers, the instability wavelength has a divergence at a finite PS layer thickness that depends on d (SiO). Using eq 9, the λ versus h data in (a) can be plotted in terms of the second derivative of the interface potential with respect to the film thickness ϕ'' in (b). The lines in (a) and (b) are fits to eq 9, with $\phi(h) = c/h^8 + \phi_{\text{vdW}}(h)$, where the first term is a short-ranged contact potential. The integration of the fitted lines gives rise to the reconstructed interfacial potentials shown in (c). The crosshatched box indicates the error of the procedure. Adapted from ref. 24.

forces. In the absence of additional forces, the experimental results can, in fact, be used to determine the Hamaker constant. The values of A extracted from the experiments are comparable to the predictions of eq 12, but a quantitative analysis relies on the assumption of the exclusive contribution of p_{vdW} to the film destabilization, an assumption that must be carefully verified. As described later, thermal fluctuation can give rise to interfacial pressures that are comparable to p_{vdW} . Recent work by Zhao et al.³² predicts that retardation effects may be significant for the SiO layer thicknesses used in some of the experiments.

Similar experiments and model calculations can also be found in ref. 33 and in a recent review.³⁴

EHD INSTABILITIES

van der Waals forces are relatively weak and short ranged (relevant only for $h \lesssim 15$ nm), making the quantitative analysis of these forces difficult. The quantitative connections between the pattern formation process and the forces that cause it are better established using a stronger and longer-ranged force. The induced dipole forces of dielectric boundaries in electric fields

are a good model system. The film destabilization of dielectric thin layers by electrostatic forces has been reported more than 100 years ago⁷ and is well understood for 70 years.⁵

An electric field across an interface between two dielectric media with dielectric constants ε_1 and ε_2 gives rise to interfacial displacement charges, which stem from the uncompensated dipole moments at the interface. The displacement charge field gives rise to an interfacial pressure. It can be derived in terms of the electrostatic energy stored in the capacitor.³⁵ For a constant applied voltage U

$$F = \frac{1}{2}CU^2 \quad (14)$$

where the capacity C is obtained by summation over the layers of material between the two electrodes. The variation of F with respect to the local film height h per unit area yields the interfacial pressure induced by the electric field.

$$p_{\text{es}} = -\varepsilon_0(\varepsilon_2 - \varepsilon_1)E_1E_2 \quad (15)$$

with ε_0 the dielectric permittivity of the vacuum, ε_1 and ε_2 the dielectric constants of the two materials, and E_1 and E_2 the electric field in the two layers (e.g., air and polymer), respectively.

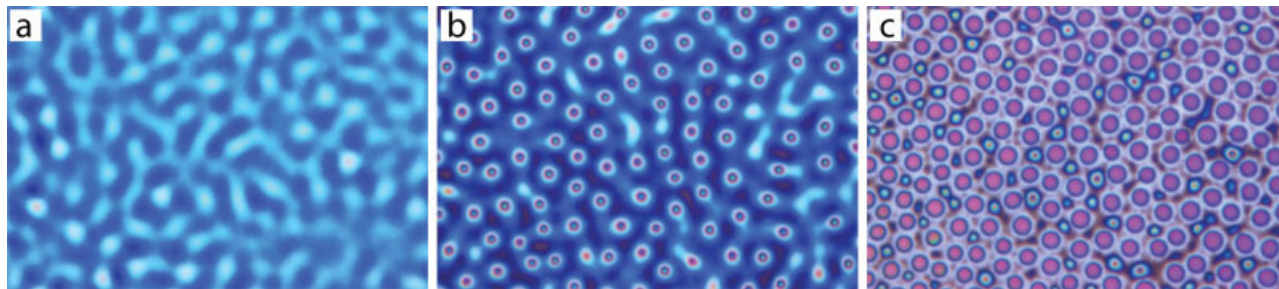


Figure 3. EHD instability of a ≈ 100 -nm thick brominated PS film. The sample was annealed inside a capacitor gap at 164°C for ≈ 20 h at an applied voltage of 40 V. The capacitor plate spacing varied from ~ 500 nm in (a) to 387 nm in (c). Because of the corresponding variation in electric field strength, different stages of the instability can be seen on the same sample: (a) early stage surface undulations; (b) undulations with wave maxima that nearly bridge the capacitor gap; and (c) late stage morphology showing columns that span the two electrodes. The data is courtesy of Harkema.³⁶ [Color figure can be viewed in the online issue, which is available at www.interscience.wiley.com.]

Equations 9 and 15 determine the pattern selection caused by the electric field

$$\lambda = 2\pi c_e \sqrt{\frac{\gamma U}{\epsilon_0}} (E_1 E_2)^{-\frac{3}{4}} \quad (16)$$

with $c_e = |(\epsilon_1 \epsilon_2)^{1/4} / (\epsilon_2 - \epsilon_1)|$.

Equation 16 provides the basis for a measurement of the interfacial pressure caused by an electric field across a liquid–air or a liquid–liquid interface. Figure 3 shows the destabilization morphologies of a polymer/air double layer sandwiched between two silicon wafers acting as electrodes, and Figure 4 shows the variation of the destabilization wavelength *versus* the applied electric field in reduced coordinates, showing a good agreement between the experimental data and the prediction of eq 16.

It is noteworthy that in the treatment described earlier, both layers were assumed to be ideally insulating dielectrics. In this case, the interfacial pressure arises exclusively from polarization effects. Although this assumption is reasonable for model polymers, it may not hold for other experimental systems. An extension to leaky dielectrics was discussed by Russel and co-workers.^{20–22}

While this discussion repeats earlier publications on this topic, it is instructive to reemphasize the good quantitative agreement of experimental data and theoretical model in the context of the “force measurement” aspect of this article. The extremely well-known nature of the interaction of matter with electric fields gives the experiments from Figures 3 and 4 a model and calibration

character. They validate the usefulness of eq 9 for the quantitative measurement of interfacial forces. The observation of amplified surface waves on micrometer length scales is therefore a powerful way of elucidating the nature of the forces that cause them.

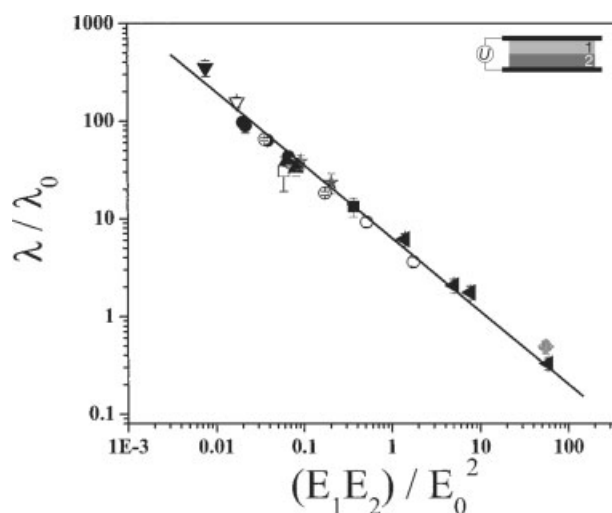


Figure 4. Variation of the instability wavelength λ with the applied electric field in a dimensionless representation. E_1 and E_2 refer to the electric fields in the upper and layer, respectively. $\lambda_0 = \epsilon_0 U^2 (\epsilon_1 - \epsilon_2)^2 / (\gamma \sqrt{\epsilon_1 \epsilon_2})$ is a reference wavelength and $E_0 = U / \lambda_0$ is a reference electric field. The symbols correspond to the instabilities measured for four polymer–polymer and five polymer–air bilayers (the details of the samples are given in ref. 13,16). In this representation, all data collapses to a master curve, which is quantitatively described by eq 16 in the absence of any adjustable parameters. The inset shows a schematic drawing of the experimental set-up. Adapted from ref. 16.

FORCES CAUSED BY THERMAL NOISE

The previous section discussed example of an experiment in which the destabilizing interfacial force was known. More importantly, eq 9 can also be used to detect less well-known (or only postulated) interfacial forces.

To motivate our discussion, the physical origin of van der Waals forces and their relationship to the Casimir effect are first reviewed. In 1948, Casimir predicted a force between two metallic plates separated by a small gap.³⁷ The plate attraction is caused by the exclusion of zero-point electromagnetic modes with wavelengths larger than two times the gap spacing. Qualitatively, the Casimir effect can be described from two different viewpoints. First, invoking a photon picture, the excluded long wavelength modes inside the gap give rise to an uncompensated radiation pressure of the electromagnetic noise that is reflected from the plate surfaces (*i.e.*, more modes are reflected from the outside surfaces of the plates, compared with the surfaces facing the gap).³⁸ A second explanation arises from the entropy of the fluctuation field. The enlargement of the external, unconfined space by reducing the gap size maximizes the number of allowed electromagnetic modes. The attractive force is therefore a consequence of the associated entropy increase. In 1961, Dzyaloshinskii et al. extended the Casimir theory to any choice of confining and confined materials, providing the base for a quantitative description of van der Waals forces, which they describe in terms of the modification of the electromagnetic zero-point noise by confinement.³⁹

In their seminal 1961 publication, they also speculated about an analogous force that may be caused by thermal noise in a confined liquid, that is, by the confinement of phonons, rather than the confinement of photons, which gives rise to van der Waals forces. This was the starting point of a highly controversial discussion about the question, whether forces in liquids can arise from thermal noise.⁴⁰ One publication asserts that forces induced by the confinement of the phonon spectrum in thermal equilibrium do not exist.⁴¹

We argue, however, that in some special cases thermal acoustic noise may indeed give rise to measurable interfacial forces. The important difference between phonons and photons in a confined liquid is their coherence length, which is much larger for electromagnetic radiation than

for molecular motion. Confinement-induced (Casimir-like) forces require a coherence length that is significantly larger than the confinement length. This requirement is not fulfilled for most liquids at finite (e.g., ambient) temperatures. Exceptions are, however, liquids at temperatures sufficiently close to their glass transition temperature (glass forming liquids). In these liquids, the molecular motion is strongly damped. While highly viscous at low frequencies, these liquids show a glassy behavior at high enough mechanical excitation frequencies. Polymer melts are typical examples of glass forming liquids.⁴² The frequency dependent rheology of polymers arises from the entangled nature of the chains in the melt. If a steady state force is applied for long enough times, individual chains have sufficient time to disentangle from their immediate neighbors. This gives rise to the viscous flow of the melt. At high enough excitation frequencies, the entanglements prevent the response of the chains on the time-scale of the excitations, and the melt shows a glassy dynamics. This is a well documented universal behavior of polymer melts. The acoustic modes of the thermal noise lie predominantly in the high frequency glass-like regime. At the frequencies that correspond to acoustic wavelengths of several nanometers (which is the confinement length scale that is of interest here), phonons in glassy polymers have correlation length of several micrometers.^{43,44} It is therefore interesting to explore whether the forces induced by the confinement of thermally excited phonons are measurable and significant.

Although a quantitative theory of this effect is complex (and to date unavailable), the order of magnitude of the effect can be estimated in two ways. Dzyaloshinskii et al.³⁹ gave the magnitude of the phonon-induced pressure in a liquid confined by two plates in terms of a scaling argument. Neglecting retardation, the effect of the confinement of electromagnetic noise is given by eq 10, which is characterized by a characteristic energy that is given by the Hamaker constant A . Since the phonon energy scale is kT per mode (k , the Boltzmann constant), a dimensional analysis suggest that the confinement of a liquid between two plates at a distance h should give rise to an attractive pressure of $p_{\text{ph}} \propto kT/h^3$ that arises from the change in the thermal mode spectrum in the liquid compared to the unconfined case.

The same relationship can also be obtained in a more direct fashion.^{45,46} Similar to the approach by Casimir, p_{ph} can also be obtained by

summing up and comparing confined and unconfined modes. Assuming a symmetrical confinement of a liquid medium (2) between two plates of medium (1)

$$p_{\text{ph}} = \frac{1}{3} \left[\int_0^{v_{\text{D}}^{(1)}} kT \, dn_1 - \int_{v_c}^{v_{\text{D}}^{(2)}} kT \, dn_2 \right] \quad (17)$$

$v_{\text{D}}^{(1)}$ and $v_{\text{D}}^{(2)}$ are the Debye frequencies of medium (1) and (2) respectively, and v_c is the lower cut-off frequency that arises from the confinement $v_c = u_2/2h$. The prefactor of $1/3$ reflects that phonons are confined only in one spatial dimension. The argument of the two integrals reflects the energy per mode of kT , and dn_1 and dn_2 are the density of states in the two media. Equation 17 can be analyzed assuming a Debye density of states for both media: $dn_i = 4\pi v^2/u_i^3 dv$, where i enumerates the two media, (1) and (2) and u_i is the velocity of sound in both media. This yields

$$p_{\text{ph}} = \frac{\pi}{18} \frac{kT}{h^3} + p_0 \quad (18)$$

where p_0 is an integration constant that does not depend on h .

Although derived in a more elaborate way than the scaling result, eq 18 is by no means more precise. Since the derivation is based on a number of simplifying assumptions (given in ref. 45), not too much importance should be attached to the prefactor of $\pi/18$.

A preliminary analysis of eq 18 shows the prediction of a very weak force that decays rapidly with increasing h . It is instructive, however, to compare eqs 10 and 18. Their same mathematical form is not surprising, since they arise from similar concepts—the confinement of photon and phonon noise spectra, respectively. Interestingly, despite the differing physical origin, both equations have similar energy scales: for commonly studied polymer films on substrates A is in the range 10^{-21} – 10^{-20} J, comparable to kT for the usual temperature range of polymer experiments. This gives rise to the surprising conclusion that eqs 10 and 18 not only have the same functional form but are also of similar magnitude.

While this means, on the one hand, that p_{ph} is not negligible and has to be taken into account whenever van der Waals forces are relevant, the similarity of the two equations also poses an experimental challenge: how to distinguish between p_{vdW} and p_{ph} ?

There are two strategies by which the two type of Casimir forces can be distinguished.⁴⁷ The first

strategy concerns the role of the temperature. While p_{vdW} is only very weakly temperature dependent (arising mainly from the first term in eq 12, which contributes only $\sim 10\%$ to the value of A), p_{ph} varies linearly with temperature. The overall temperature range over which this can be probed is small, however, delimited by the glass transition and the temperature of thermal degradation of the polymer. A second approach concerns the role of the boundary conditions. Electromagnetic confinement requires a large enough difference in dielectric properties of the confined and confining media. In terms of eq 12, this implies that the refractive index of the confined liquid must be sufficiently different from those of the confining walls. For the confinement of phonons, the confined medium must have mechanical properties (i.e. a Young's modulus) that are sufficiently different from that of the confining walls.

In analogy to the studies of film destabilization by electric fields, a convenient experimental approach to detect p_{ph} is the study of stability of supported thin polymer films.⁴⁷ The first experimental approach addresses the temperature variation of the spontaneous amplification of capillary waves. To this end, the sample configuration described in the “van der Waals Forces” section was used: a low molecular weight PS film supported on silicon wafer that had a 1.6-nm thick native oxide layer. As described earlier, the effective Hamaker constant that takes the oxide layer into account changes sign as the film thickness is increased. In particular, there is a crossover in film thickness h_c , where $p_{\text{vdW}} \approx 0$. The phonon-induced pressure p_{ph} is, on the other hand, not influenced by the presence of the oxide layer (both, the oxide and the silicon substrate have Young's moduli that are significantly higher compared to the polymer). It has a destabilizing effect on the film for all thicknesses.

Since test experiments require the manufacture of 1–10 nm thick films, polymers (oligomers) with low molecular weights were used (~ 2 kg/mol). In the melt, these polymers have a radius of gyration of ≈ 1 nm, which is smaller than the relevant film thickness of these experiments (2–10 nm). As opposed to longer polymers, where the confinement of the chains below their radius of gyration may come into play, we expect forces that arise from an entropy loss of the chains due to the confinement of the polymer in the film or at one of the surfaces to be negligible.

Figure 5(a,b) shows atomic force microscopy (AFM) images of thin PS films (molecular weight

$M_w = 1.92$ kg/mol). The 2.4-nm thick film, which was annealed for 15 min at 50 °C, shows the signature of a spontaneously amplified wave with a well-defined mode λ [Fig. 5(a)]. Increasing the film thickness by 1.3 nm resulted in a film that was stable for many hours at a temperature of 50 °C. When raising the temperature to 170 °C, isolated holes were formed [Fig. 5(b)]. This sample morphology is due to the film break-up by heterogeneous nucleation, which is an indication that the film is stable with respect to capillary surface waves. The crossover film thickness h_c must therefore lie between 2.4 and 3.7 nm.

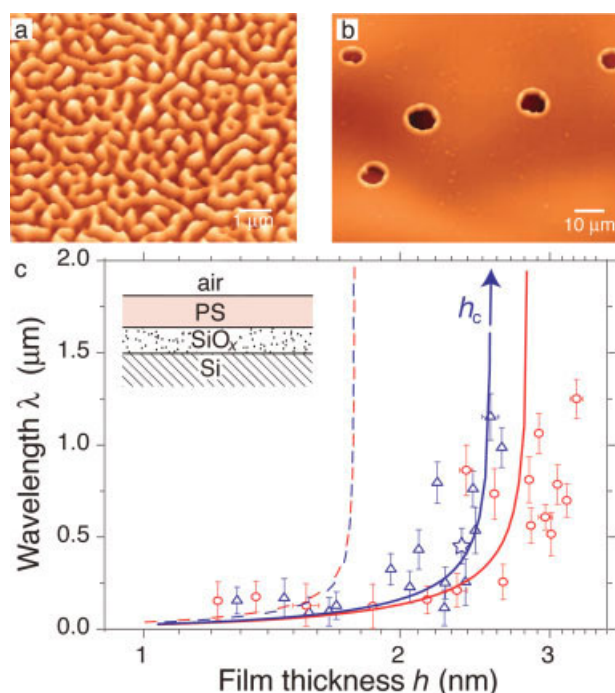


Figure 5. Temperature dependence of the instability of PS films on Si substrates, which were covered by a 1.6-nm thick oxide layer. The 2.4-nm thick film in (a) showed a capillary instability after annealing for 15 min at 50 °C, while a 3.7-nm thick film stayed stable for many hours at this temperature. The film broke up only *via* a different mechanism, the nucleation of holes, after raising the temperature to 170 °C (b). (c) Variation of λ versus h for two different annealing temperatures. Raising the annealing temperature from 50 to 170 °C causes a shift of the λ divergence from $h_c \approx 2.4$ nm to $h_c \approx 3$ nm. This corresponds to an increase in the overall destabilizing pressure gradient, which cannot be explained by van der Waals forces alone. The star corresponds to the data extracted from (a). Adapted from ref. 47. [Color figure can be viewed in the online issue, which is available at www.interscience.wiley.com.]

A systematic study of this effect is shown in Figure 5(c) for two annealing temperatures, 50 and 170 °C. Both data sets show increasing instability wavelengths λ with increasing film thickness that diverge at a critical film thickness h_c . Despite the scatter in the data, the value of h_c at 170 °C is clearly higher compared with the lower temperature data set.

The data from Figure 5(c) can be analyzed in terms of eq 9, taking $p_{\text{int}} = p_{\text{vdW}} + p_{\text{ph}}$. The inclusion of both terms results in a good qualitative description of the data. A model using $p_{\text{int}} = p_{\text{vdW}}$ is also shown (dashed and dotted lines), using calculated values of A based on eq 12. A model that is exclusively based on van der Waals forces clearly does not reflect the experimental data.

In a second experimental approach, the electromagnetic boundary condition was varied. By matching the refractive indices of film and substrate, A can be made very small. This is shown for two experimental systems in Figure 6. In these experiments, substrates with slightly higher refractive indices than the films were chosen. According to eq 12, this results in small, negative values of A , and therefore in contributions of p_{vdW} , which weakly stabilize the film. For these sample parameters p_{ph} has a destabilizing effect on the film, with a larger magnitude than p_{vdW} .

The results for polymethylmetacrylate (PMMA, $M_w = 2.5$ kg/mol, $n = 1.49$) on glass ($n = 1.52$) and polyacrylamide (PAAM, $M_w = 1.52$ kg/mol, $n = 1.45$) on thermally grown silicon oxide ($n = 1.46$) are shown in Figure 6(a,b). Even though a negative value of A (corresponding to a negative value of p_{vdW}) is predicted for both the systems, the films show clear signs of spontaneous film instabilities. Since a negative sign of p_{vdW} implies a stabilizing effect of the van der Waals forces, the instability observed in Figure 6(a,b) are a clear signature of p_{ph} , which overpowers the stabilizing effect of the van der Waals forces. This is confirmed by the systematic study in Figure 6(c,d). The solid lines are the predictions of eq 9 with $p_{\text{int}} = p_{\text{vdW}} + p_{\text{ph}}$ (using $p_{\text{int}} = p_{\text{vdW}}$ does not give a real solution of eq 9).

Using glass as a substrate for PMMA films has the advantage that the refractive index (and therefore the value of A) can be varied by doping the glass with metals. Glasses with a range of refractive indices are commercially available. PMMA films were found to be unstable on glass substrates with values of n in the range 1.5–1.6. Films on glass with $n = 1.71$, on the other hand, were stable. Obviously, for $n = 1.71$, the stabiliz-

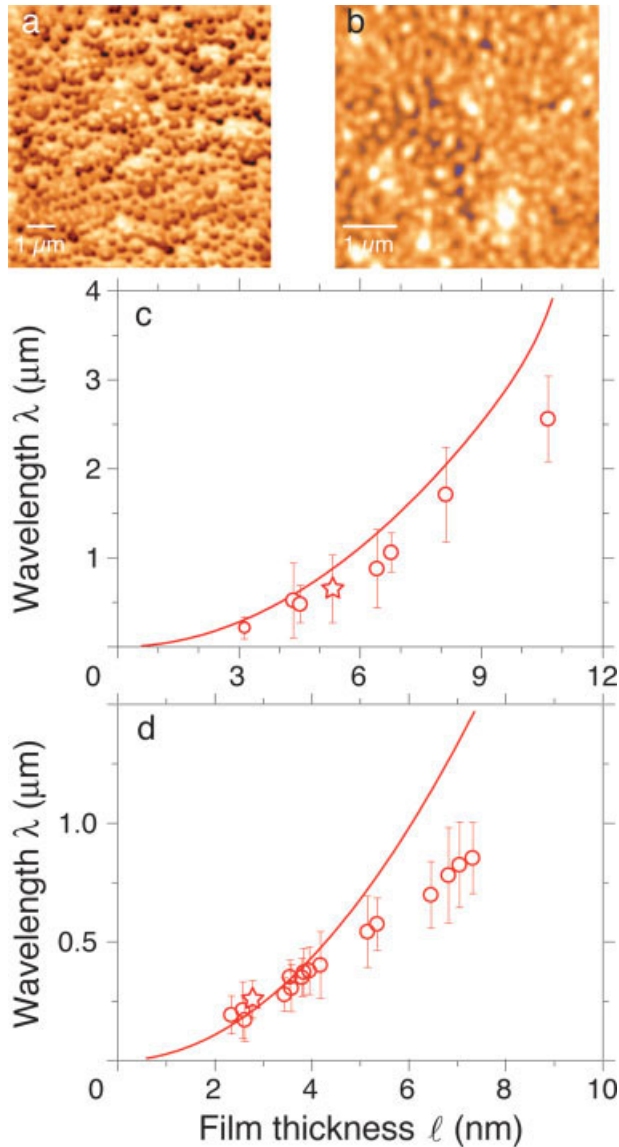


Figure 6. Destabilization of polymer films in the presence of weakly stabilizing van der Waals forces. (a) PMMA ($n = 1.49$) on glass ($n = 1.52$), annealed at $130\text{ }^{\circ}\text{C}$, and (b) PAAM ($n = 1.45$) on silicon oxide ($n = 1.46$), annealed at $170\text{ }^{\circ}\text{C}$. Both films are predicted to be stable based on a van der Waals argument alone. (c) and (d) show the variation of λ versus h for the two systems. The stars correspond to (a) and (b) and the lines are predictions from eq 9 with $p_{\text{int}} = p_{\text{vdW}} + p_{\text{ph}}$. Adapted from ref. 47. [Color figure can be viewed in the online issue, which is available at www.interscience.wiley.com.]

ing effect of p_{vdW} was stronger than the destabilization by p_{ph} .

A third experimental strategy involves the modification of the mechanical boundary condition of the film. The approach of eq 17 is valid

only if the mode spectra of the film and the surrounding media are fully decoupled. This implies that the elastic moduli of the film and the surrounding materials have to be sufficiently different. This is the case for polymers on hard substrates, such as silicon, with elastic moduli that differ by two orders of magnitude. Choosing substrates that have mechanical properties similar to those of the film removes the phonon confinement, since the elastic modes of film and substrate are coupled.

To test the response of the film instability on a change in the mechanical boundary condition, substrates with similar optical properties (and

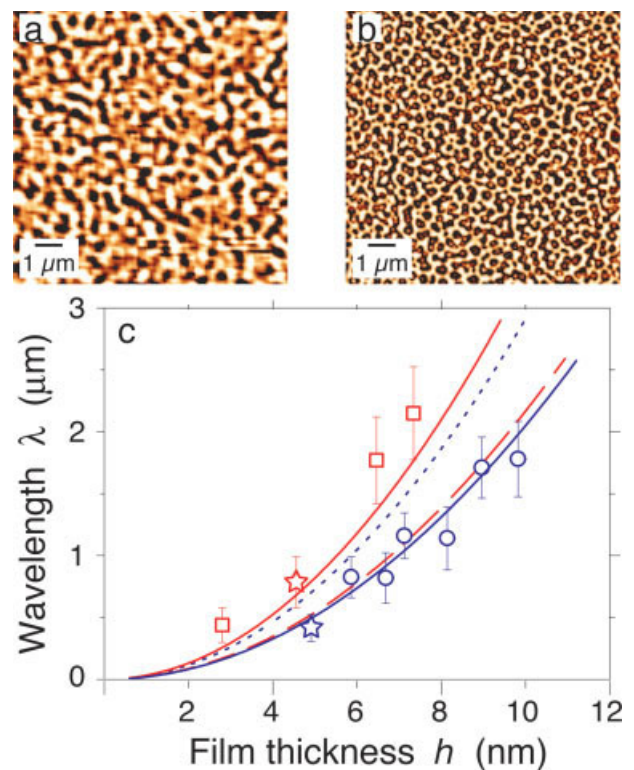


Figure 7. Stability of $\approx 4.7\text{-nm}$ thick PS ($n = 1.59$) films on (a) PMMA ($n = 1.49$) and (b) silicon oxide ($n = 1.48$) surfaces. Despite the similar film thicknesses and optical substrate parameters, there is a clear difference in the film morphology, which is an indication for differing destabilizing pressures. In (c), eq 9 for PS on PMMA (squares) gives a better prediction when assuming $p_{\text{int}} = p_{\text{vdW}}$ (solid line) as opposed to $p_{\text{int}} = p_{\text{vdW}} + p_{\text{ph}}$ (dashed line). The opposite applies for PS films on silicon oxide (circles). Taking $p_{\text{int}} = p_{\text{vdW}} + p_{\text{ph}}$ (solid line) gives a better prediction for this data set compared to the effect of van der Waals forces alone ($p_{\text{int}} = p_{\text{vdW}}$, dotted line). The stars correspond to (a) and (b). Adapted from ref. 47. [Color figure can be viewed in the online issue, which is available at www.interscience.wiley.com.]

therefore similar values of A , see eq 12), but different elastic properties, were chosen. Figure 7 shows the comparison of PS ($n = 1.59$) film instabilities on a silicon oxide [Fig. 7(a)] and a PMMA [$M_w = 1080$ kg/mol, Fig. 7(b)] substrate. Both substrates have similar refractive indices (1.48 and 1.49, respectively). The layers are therefore exposed to very similar values of p_{vdW} . The visual inspection of two ~ 4.7 -nm thick PS films that were annealed for several minutes at 90°C shows a much smaller destabilization wavelength λ for PS on SiO_x compared to PS on PMMA. Clearly, the overall destabilizing pressure of the PMMA film on SiO_x was significantly higher compared with PS on PMMA. Since PS and PMMA have very similar elastic moduli, the phonon density of states of film and substrate are coupled. Film destabilization is driven only by the van der Waals forces ($p_{int} = p_{vdW}$), whereas PS on a higher elastic modulus substrate is driven by the combined effect of both confinement induced pressures ($p_{int} = p_{vdW} + p_{ph}$). This is borne out by the more systematic study shown in Figure 7(c). The values of λ for PS on SiO_x lie systematically below those for PS on PMMA. Both data sets are well described by eq 9, with $p_{int} = p_{vdW}$ for the PS on PMMA data set and $p_{int} = p_{vdW} + p_{ph}$ for the PS on SiO_x data sets, respectively.

The complementary experiment is the investigation of films with a refractive index that is lower compared to the substrate. Also here, two substrates with similar optical but different mechanical properties were used. PMMA ($n = 1.49$) was deposited onto PS ($M_w = 2057$ kg/mol, $n = 1.59$) and glass ($n = 1.61$) substrates. As before, we expect that the matched mechanical properties of PS and PMMA result in a significant reduction of the phonon confinement. Since the refractive index of the film is lower than those of the substrates, films are stabilized by the van der Waals pressure ($p_{vdW} < 0$). Comparing ~ 5.7 -nm thick PMMA films on the two different substrates after annealing for several minutes at 110°C , a striking difference is revealed. PS on glass in Figure 8(a) remained stable, while PS on PMMA in Figure 8(b) showed a characteristic undulatory instability. This is readily explained in terms of the balance of p_{vdW} and p_{ph} . The exclusive contribution of p_{vdW} in Figure 8(a) stabilizes the film, while the overall pressure $p_{int} = p_{vdW} + p_{ph}$ in Figure 8(b) is dominated by the destabilizing effect of p_{ph} . In this case, the variation of λ versus film thickness is qualitatively described by eq 9, shown in Figure 8(c).

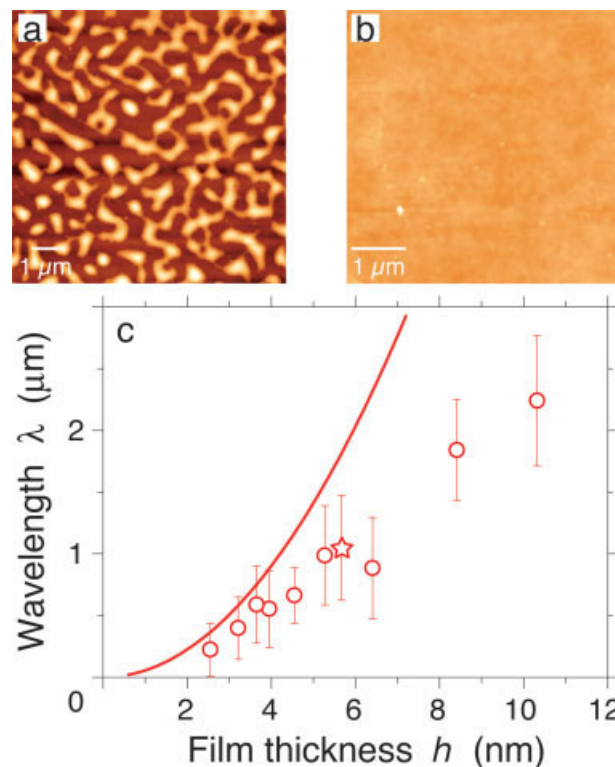


Figure 8. Stability of ~ 5.7 -nm thick PMMA ($n = 1.49$) films on (a) high refractive index glass ($n = 1.61$) and (b) PS ($n = 1.59$) surfaces. Only PMMA on PS is stable, which is an indication for a stabilizing disjoining pressure. The data in (c) corresponds to samples similar to the one shown in (a) (star). The solid line is the prediction of eq 9 with $p_{int} = p_{vdW} + p_{ph}$. Adapted from ref. 47. [Color figure can be viewed in the online issue, which is available at www.interscience.wiley.com.]

CONCLUSIONS

The purpose of this review is to demonstrate that the observation of spontaneously destabilizing thin films can be used to quantitatively deduce the interfacial forces that cause the instability. This provides a simple but powerful way to map out forces on the length scale of a few nanometers. The SJH approach²⁴ shows that parameters that are observable in a straight forward fashion (the characteristic wavelength *vs.* the film thickness) can be used to reconstruct the spatial variation of the effective interface potential. By using dielectric materials in electric fields, which are characterized by interactions that are well understood, it is possible to show that the instability is quantitatively described by a simple model, which is based on a linear stability analysis. The third example shows that by the systematic variation of sample param-

eters it is possible to detect and characterize an interfacial force that is caused by the confinement of the phonon density of states in thin polymer films. This provides a rare experimental contribution to the hotly debated question, whether a modification of the phonon spectrum in liquids can give rise to measurable forces. A further example, how spontaneously amplified film instabilities can be used to characterize a hitherto unknown interfacial force (also caused by phonons) can be found in two recent reviews.^{48,49}

REFERENCES AND NOTES

- Lord Rayleigh, J. W. S. *Proc Lond Math Soc* 1878, 10, 4–13.
- Lord Rayleigh, J. W. S. *Philos Mag* 1892, 34, 145–154.
- Vrij, A. *Discuss Faraday Soc* 1966, 42, 23–33.
- Brochard-Wyart, F.; Dailant, J. *Can J Phys* 1990, 68, 1084–1088.
- Melcher, J. R. *Field-Coupled Surface Waves*; MIT Press: Cambridge, 1963.
- Lord Rayleigh, J. W. S. *Philos Mag* 1882, 14, 187.
- Swan, J. W. *Proc R Soc London* 1897, 62, 38–46.
- Gundlach, R. W.; Claus, C. J. *Photogr Sci Eng* 1963, 7, 14.
- Urbach, J. C.; Meier, R. W. *Appl Opt* 1966, 5, 666.
- Chou, S. Y.; Zhuang, L.; Guo L. *Appl Phys Lett* 1999, 75, 1004–1006.
- Chou, S. Y.; Zhuang, L. *J Vac Sci Tech* 1999, 17, 3197–3202.
- Schäffer, E.; Thurn-Albrecht, T.; Russell, T. P.; Steiner, U. *Nature* 2000, 403, 874–877.
- Schäffer, E.; Thurn-Albrecht, T.; Russell, T. P.; Steiner, U. *Europhys Lett* 2001, 53, 518–524.
- Morariu, M. D.; Voicu, N. E.; Schäffer, E.; Lin, Z.; Russell, T. P.; Steiner, U. *Nat Mater* 2003, 2, 48–52.
- Lin, Z.; Kerle, T.; Baker, S. M.; Hoagland, D. A.; Schäffer, E.; Steiner, U.; Russell, T. P. *J Chem Phys* 2001, 114, 2377–2381.
- Lin, Z.; Kerle, T.; Russell, T. P.; Schäffer, E.; Steiner, U. *Macromolecules* 2002, 35, 3971–3976.
- Lin, Z.; Kerle, T.; Russell, T. P.; Schäffer, E.; Steiner, U. *Macromolecules* 2002, 35, 6255–6262.
- Shankar, V.; Sharma, A. *J Colloid Interface Sci* 2004, 274, 294–308.
- Verma, R.; Sharma, A.; Kargupta, K.; Bhaumik, J. *Langmuir* 2005, 21, 3710–3721.
- Pease, L. F., III; Russel, W. B. *J Non-Newtonian Fluid Mech* 2002, 102, 233–250.
- Pease, L. F., III; Russel, W. B. *J Chem Phys* 2003, 118, 3790–3803.
- Pease, L. F., III; Russel, W. B. *Langmuir* 2004, 20, 795804.
- Wu, N.; Russel, W. B. *Appl Phys Lett* 2005, 86, 241912.
- Seemann, R.; Herminghaus, S.; Jacobs, K. *Phys Rev Lett* 2001, 86, 5534–5537.
- Schäffer, E.; Harkema, S.; Roerdink, M.; Blossey, R.; Steiner, U. *Adv Mater* 2003, 15, 514–517.
- Harkema, S.; Schäffer, E.; Morariu, M. D.; Steiner, U. *Langmuir* 2003, 19, 9714–9718.
- Langbein, D. *Capillary Surfaces*; Springer: Berlin, 2002.
- Batchelor, G. K. *An Introduction to Fluid Dynamics*; Cambridge University Press: Cambridge, England, 1967.
- Israelachvili, J. N. *Intermolecular and Surface Forces*; Academic Press: London, 1991.
- Visser, J. *Adv Colloid Interface Sci* 1972, 3, 331–363.
- Müller, M.; MacDowell, L. G.; Müller-Buschbaum, P.; Wunnike, O.; Stamm, M. *J Chem Phys* 2001, 115, 9960–9969.
- Zhao, H.; Wang, Y. J.; Tsui, O. K. C. *Langmuir* 2005, 21, 5817–5824.
- Müller-Buschbaum, P.; Wunnicke, O.; Stamm, M.; Lin, Y.-C.; Müller, M. *Macromolecules* 2005, 38, 3406–3413.
- Seemann, R.; Herminghaus, S.; Neto, C.; Schlagowski, S.; Podzimek, D.; Konrad, R.; Mantz, H.; Jacobs, K. *J Phys: Condens Matter* 2005, 17, S267–S290.
- Schäffer, E. *Instabilities in Thin Polymer Films: Structure Formation and Pattern Transfer*. Ph.D. Thesis, University of Konstanz, Konstanz, Germany, Sept. 2001.
- Harkema, S. *Instabilities in Thin Polymer Films: Insights in Structure Formation and Pattern Replication*. Ph.D. Thesis, University of Groningen, Groningen, The Netherlands, Sept. 2005.
- Casimir, H. B. G. *Proc K Ned Akad Wet* 1948, 51, 793.
- Milonni, P. W.; Cook, R. J.; Goggin, M. E. *Phys Rev A* 1988, 78, 1621–1634.
- Dzyaloshinskii, I. E.; Lifshitz, E. M.; Pitaevskii, L. P. *Adv Phys* 1961, 10, 165–209.
- Jones, R. B. *Physica (Amsterdam)* 1981, 105, 395–416.
- Chan, D. Y. C.; White, L. R. *Physica (Amsterdam)* 1983, 122, 505–515.
- Strobl, G. *The Physics of Polymers*; Springer: Berlin, 1997.
- Morath, C. J.; Maris, H. J. *Phys Rev B* 1996, 54, 203–213.
- Behrends, R.; Kaatze, U. *J Phys Chem A* 2000, 104, 3269–3275.
- Schäffer, E.; Steiner, U. *Eur Phys J E Soft Matter* 2002, 8, 347–351.
- Morariu, M. D.; Schäffer, E.; Steiner, U. *Eur Phys J E Soft Matter* 2003, 12, 375.
- Morariu, M. D.; Schäffer, E.; Steiner, U. *Phys Rev Lett* 2004, 92, 156102.
- Steiner, U. In *Nanoscale Assembly—Chemical Techniques*; Huck, W. T. S., Ed.; Springer: Berlin, 2005; Vol. 8, pp 1–24.
- Steiner, U. In *Non-Conventional Lithography and Patterning: Techniques and Application*; Bucknall, D. G., Ed.; Woodhead Publishing: Cambridge, 2005.